Numerical study on THz radiation of two-dimensional plasmon resonance of GaN HEMT array

Hongyang Guo(郭宏阳), Ping Zhang(张平), Shengpeng Yang(杨生鹏),
Shaomeng Wang(王少萌), and Yubin Gong(宫玉彬)†

National Key Laboratory of Science and Technology on Vacuum Electronics, University of Electronic Science and Technology of China, Chengdu 610031, *China*

(Received 4 November 2022; revised manuscript received 26 December 2022; accepted manuscript online 6 January 2023)

The GaN high electron mobility transistor (HEMT) has been considered as a potential terahertz (THz) radiation source, yet the low radiation power level restricts their applications. The HEMT array is thought to improve the coupling efficiency between two-dimensional (2D) plasmons and THz radiation. In this work, we investigate the plasma oscillation, electromagnetic radiation, and the integration characteristics of GaN HEMT targeting at a high THz radiation power source. The quantitative radiation power and directivity are obtained for integrated GaN HEMT array with different array periods and element numbers. With the same initial plasma oscillation phase among the HEMT units, the radiation power of the two-element HEMT array can achieve 4 times as the single HEMT radiation power when the array period is shorter than 1/8 electromagnetic wavelength. In addition, the radiation power of the HEMT array varies almost linearly with the element number, the smaller array period can lead to the greater radiation power. It shows that increasing the array period could narrow the main radiated lobe width while weaken the radiation power. Increasing the element number can improve both the radiation directivity and power. We also synchronize the plasma wave phases in the HEMT array by adopting an external Gaussian plane wave with central frequency the same as the plasmon resonant frequency, which solves the problem of the radiation power reduction caused by the asynchronous plasma oscillation phases among the elements. The study of the radiation power amplification of the one-dimensional (1D) GaN HEMT array provides useful guidance for the research of compact high-power solid-state terahertz sources.

Keywords: GaN HEMT array, two-dimensional (2D) plasmons, THz emission

PACS: 07.57.Hm, 42.72.Ai **DOI:** 10.1088/1674-1056/acb0bb

1. Introduction

THz waves are believed to have great application prospects in nondestructive imaging, biological monitoring, high-speed communication, *etc*.[1–4] Thus, the realization of THz source with frequency of several THz, high radiation power and low machining difficulty has been one of the research hotspots in recent years.[5] The two-dimensional plasmons (2DPs) formed in two-dimensional electron gas (2DEG) in field-effect transistors (FETs) have long been considered to produce THz radiation,[6,7] and THz plasmonic semiconductor devices are considered as potential solutions for miniaturized and integrated THz emission.[8,9] As one of the representative THz emission theories, Dyakonov–Shur (DS) instability theory demonstrates that the plasma instability occurs and produces far-infrared (FIR) radiation under asymmetric boundary conditions in an HEMT.[10] After that, various microwave/THz management emitters or detectors based on plasma oscillations within semiconductor heterojunctions have been extensively investigated. Among them, THz radiation experiments of high electron mobility transistors (HEMTs) were carried out with different structures that convert plasma wave into electromagnetic radiation including single metal gates,[11–13] grating gates,[14–16] and dual grating gates.[17–20] In grating gate HEMT, the electron density in 2DEG and plasma wave velocity distribute periodically, consequently periodic plasmonic resonant cavity form in the channel, the boundary conditions of the cavity are determined by its both sides of gate voltages. The grating gate HEMT were thought to produce greater plasma instability and electromagnetic radiation compared with the single metal strip gate.[21]

Another type of periodized plasmonic cavities are formed in the channel directly by integrating HEMTs into 1D or 2D arrays on the same active layer. Shur *et al*. proposed a device where a plurality of FETs were formed on the same active layer and the gate, source and drain contacts of the FETs were connected to one or more connectors,[22] this device can be used to generate, mix, or detect THz radiation. The FETs in the array can work independently or dependently. Elkhatib *et al*. found HEMTs connected in series could greatly enhance the detector responsivity, and the responsivity is proportional to the element number of the array.[23] Popov *et al*. found that FET array could effectively improve the coupling efficiency between THz waves and 2D plasmons in the channel.[24] Besides the advantages of enhanced responsivity of the FET array as a THz detector, the FET array as a THz emitter has not yet been studied in detail.

Under asymmetric boundary conditions, FET behaves as

†Corresponding author. E-mail: ybgong@uestc.edu.cn

© 2023 Chinese Physical Society and IOP Publishing Ltd

an independent terahertz source without external radiation.[10] In addition, because the channel length in the FET is much shorter than its electromagnetic radiation wavelength, the radiation characteristics of the FET array are similar to those of the element antenna array. In this work, combining the antenna array theory, the radiation directivity and power of the HEMT array are studied when the plasma waves in HEMT elements in the array are synchronously excited. The radiation directivity and radiation power of the HEMT array are researched and the influence of the array period and element number on the radiation power, radiation field shape and radiation directivity are analyzed, respectively. In order to overcome the radiated power reduction caused by the asynchronous phases of the plasma oscillations in the array, external Gaussian plane wave excitation is proposed to synchronize the phases of plasma waves in the HEMT array. The study of the THz radiation of the 1D GaN HEMT array provides another strategy to realize high power solid-state THz sources.

2. Plasmon resonance in 2DEG and THz radiation of the single GaN HEMT

In this work, the GaN and AlGaN layers with the same dielectric constant of 9.7 are in turn grown on the substrate layer, and the 2DEG is supposed to be sandwiched by GaN and AlGaN layers. The gate electrode locates on top of AlGaN layer between the source and drain electrodes. The 2D electron flow is assumed to flow in the source–drain bias direction (x direction) and the 2DEG width is considered much longer than the 2DEG length. The three-dimensional (3D) model of the GaN HEMT and the local view near the 2DEG are shown as Fig. 1.

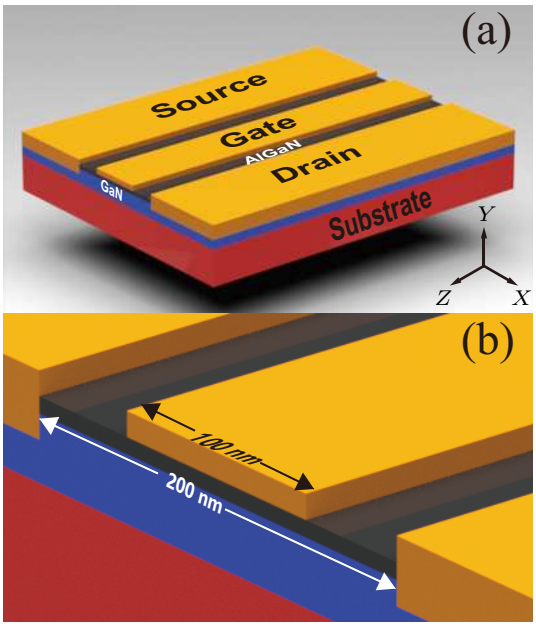


Fig. 1. The 3D model (a) and local view (b) of the GaN HEMT element.

Suppose the electron velocity along the channel is $v(x,t)$, the electron sheet density is $n(x,t)$ and $j(x,t) = n(x,t)v(x,t)$. The electron flow in the channel satisfies 1D hydrodynamic equations as shown in Eqs. (1) and (2), where m_e^* is the electron effective mass, τ_p is the 2DEG momentum relaxation time, and E_x is the electric field in x direction along the channel.

$$\frac{\partial n}{\partial t} + \frac{\partial j}{\partial x} = 0, \tag{1}$$

$$\frac{\partial j}{\partial t} + \frac{\partial jv}{\partial x} = -\frac{ne}{m_e^*}E_x - \frac{j}{\tau}. \tag{2}$$

In order to obtain the plasma oscillation in GaN HEMT and its induced electromagnetic radiation, the hydrodynamic equation satisfied by 2DEG and the Maxwell equation in XOY plane are established and solved together. The hydrodynamic equations above are coupled with Maxwell's equations in order to realize the energy exchange between the 2DPs and electromagnetic waves. The finite-difference time-domain (FDTD) methods similar to Refs. [25,26] are adopted to solve the coupled hydrodynamic equations and Maxwell's equations. As shown in Fig. 2, equations in the upper and lower half in the figure are the hydrodynamic equations and Maxwell's equations, respectively. By solving the hydrodynamic difference equation, the electron concentration and surface current density at each cell of the 2DEG can be solved. This process requires the electric field value at each cell of the 2DEG obtained by solving the Maxwell equations at the last time. As shown in the bottom box in Fig. 2, the surface current density at each node of the 2DEG is regarded as a current source and generates radiant electric and magnetic fields in the entire region. The red broken lines with arrows in Fig. 2 represent the energy exchange between the plasma oscillation and the EM field.

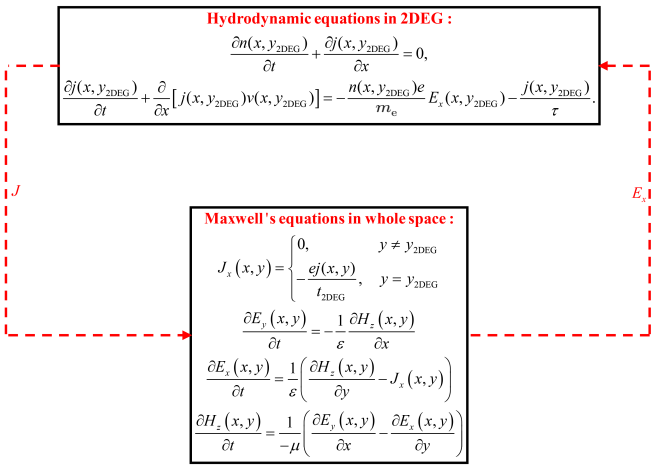


Fig. 2. Schematic diagram of hydrodynamic-Maxwell equations coupling.

Moreover, DS boundary conditions that $n = n_0$ at source and $j = n_0 v_0$ at drain are also added during the computation in the process of computing the $n(xt)$ and $j(xt)$, where n_0 is equilibrium sheet electron concentration and v_0 is DC electron velocity. The boundary condition that $n(0,t) = n_0$ means that

the AC voltage and impedance are both zero at source side. And $j(L,t)=n_0 v_0$ means that the AC impedance is infinite at drain. It has been confirmed numerically that when the electron DC velocity is not zero, the plasma wave amplification happens at the drain side under DS boundary condition.[25] In experiments, in order to achieve these boundary conditions, the source of the HEMT was grounded and the HEMT was operated in the saturated region, which ultimately proved to achieve plasma instability and THz radiation.[11] Combing equations above and the DS boundary conditions, the plasma wave oscillation in the 2DEG its induced electromagnetic field are obtained eventually.

During the computation, the electron effective mass in channel is $0.22m_0$; the source–drain spacing is 200 nm; the gate length is 100 nm; the width of the HEMT is 200 μm. The HEMT locates at center of an air box with size of 1 mm × 1 mm and the air box is wrapped by a perfect matching layer to absorb the radiation wave.

In order to achieve the DS boundary condition, the voltage between the source and drain is applied to enable the transistor operate in the saturation region.[11] Due to that the saturation velocity of the electrons in GaN/AlGaN heterojunction is about 2×10^5 m/s,[27] the electron DC velocity v_0 is set as 2×10^5 m/s during the simulation. Moreover, the electron equilibrium sheet concentration n_0 is set as 1×10^{13} cm^{-2}. The electron momentum relaxation time τ_p is set as 1 ps. The plasma instability in 2DEG in GaN HEMT are firstly achieved. The time-dependence curve of the alternative part of the source areal current density J_s are shown in Fig. 3(a), it shows that the source current oscillation increases in the first 30 ps and then reaches saturation because of the nonlinear effects of the 2D electron flow.[28] The temporal and spatial dependence of the sheet current density J in the channel is shown in Fig. 3(b), which shows that the sheet current is the strongest at source side but fixed at drain side, the plasma wave varies about 3/4 wavelength from source to drain. The frequency spectrums of J_s corresponding to different n_0 are shown in Fig. 3(c). When n_0 varies from 8×10^{12} cm^{-2} to 1.6×10^{13} cm^{-2}, the oscillation frequency of J_s increases from 6 THz to 8.6 THz. In theory, the frequency of different orders of ungated plasmons limited by DS boundary conditions are[29]

$$\omega=\sqrt{\frac{e^2n_0}{2\varepsilon mL}\left(\frac{\pi}{2}+n\pi\right)},\quad n=0,1,2,3,\ldots \tag{3}$$

As shown in Fig. 3(d), the theoretical frequencies of the second order of ungated plasma resonance ($n=1$ in Eq. (3)) are compared with the numerical frequencies corresponding to different electron concentrations n_0. The black solid line and red scatter are the theoretical values and numerical solutions of the resonant frequency respectively. It shows that the numerical solutions and theoretical values are in good agreement. The electron sheet concentration or gate voltage has a strong correlation with the resonant frequency of plasma wave.

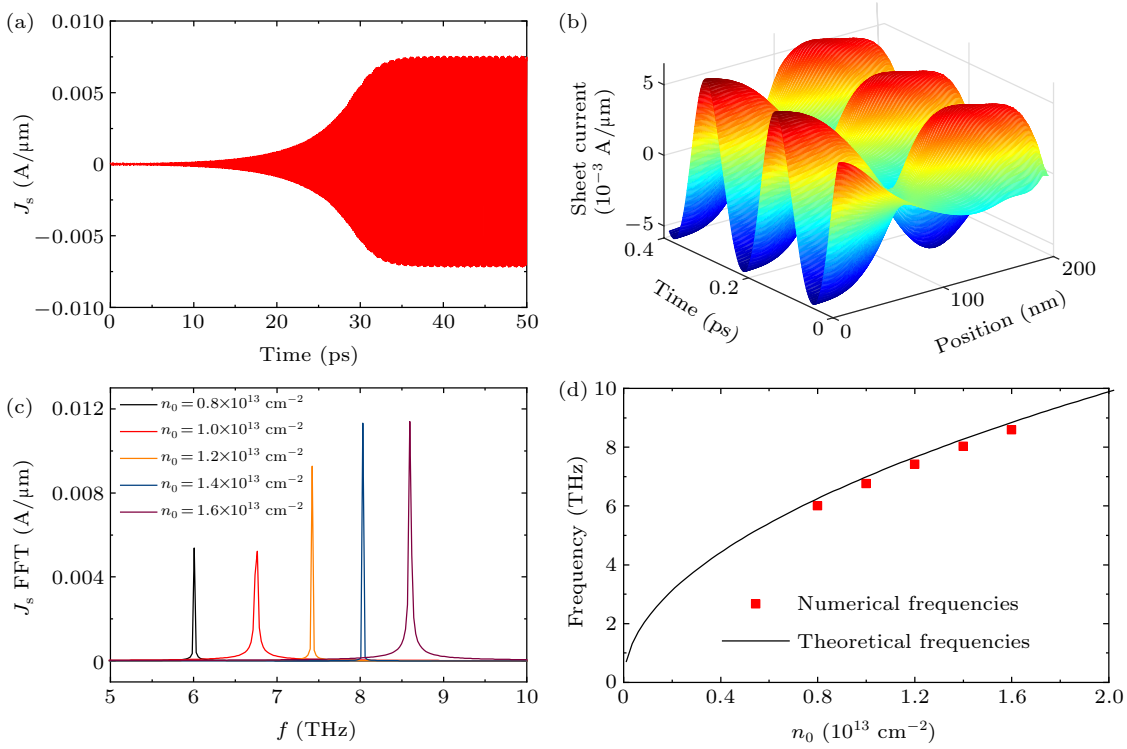


Fig. 3. (a) The temporal dependence of the source sheet current density J_s; (b) the temporal and spatial dependence of sheet current density J along the channel in the time interval of 0.2 ps after the plasma wave oscillation become saturated; (c) the spectrum of J_s corresponding to different n_0; (d) the comparison of the theoretical second ungated plasmon frequencies (black solid line) and the numerical plasma wave frequencies (red scatters) corresponding to different 2DEG sheet concentrations n_0.

In addition, the electron momentum relaxation time τ_p in GaN/AlGaN heterojunction has different values at different temperatures. τ_p decreases from 4.3 ps at 77 K to 0.28 ps at 300 K.[30] The plasma oscillation in the 2DEG when τ_p varies from 0.4 ps to 4 ps are simulated. The temporal dependences areal current density J_s at the source side corresponding to different τ_p are shown in Fig. 4. It shows that when τ_p is 0.4 ps, that is, at room temperature, J_s decays with time. When τ_p is higher than 1 ps, the growth rate and oscillation amplitude of J_s increase with the increase of τ_p. In other words, plasma instability is easier to be achieved at lower temperatures.

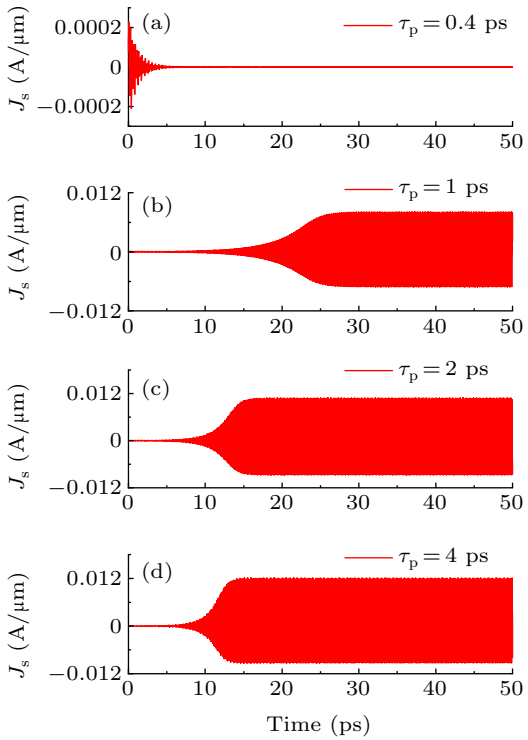


Fig. 4. The temporal dependences of the areal alternative currents at source when the electron momentum relaxation time τ_p is 0.4 ps (a), 1 ps (b), 2 ps (c), and 4 ps (d), respectively.

The electric field excited by the 2DPs is shown in Fig. 5. The 2D distribution of the electric field vector inside the HEMT is shown in Fig. 5(a), in which the black dashed line represents the 2DEG and the black blocks are the metal electrodes. The electric field near the source is horizontal and perpendicular to the side wall of the source, the gate gives rise to strong electric field normal to its side and lower walls. The electric field in the right side in the HEMT is weaker than that in the left side. As shown in Fig. 5(b), in the region of 1 mm × 1 mm, the electromagnetic radiation energy generated by the 2DPs is mainly concentrated in the tapered area on either side of the vertical line of the HEMT. Since the 2DEG length is far shorter than the wavelength of the radiation wave, therefore, the GaN HEMT can be analogous to an element antenna. The radiation power of the HEMT is computed numerically by multiplying the loop integral of Poynting vector at air boundaries and the HEMT width in z direction, the radiation power of the HEMT is 113 μW.

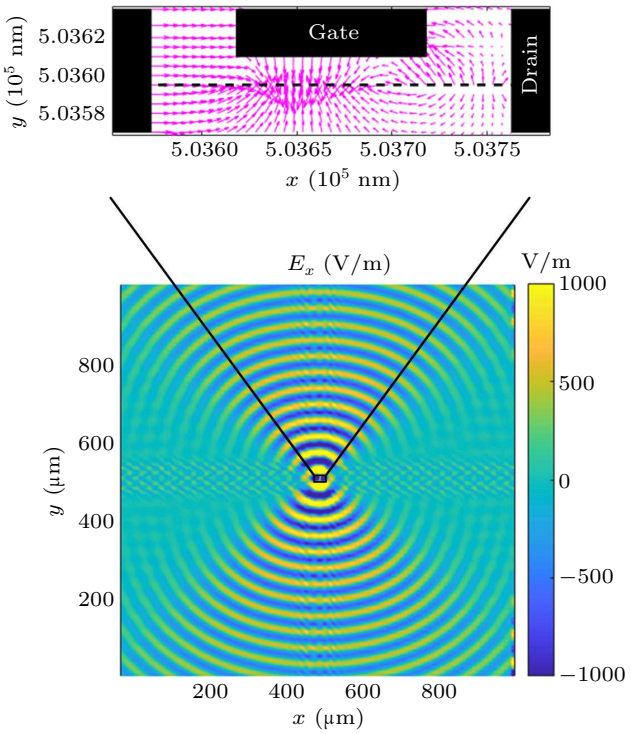


Fig. 5. (a) The 2D distribution of the electric field vector in the HEMT internal area, (b) the 2D distribution of electric field component E_x in the whole air box.

3. THz radiation of 1D GaN HEMT array with synchronous plasmon phases among the units

Due to that the radiated field of the HEMT unit is similar to that of the electric dipole, the HEMT unit can be analogized as an element antenna. Thus, with the help of array antenna theory,[31] the radiation power improvement and the radiation directivity of the of HEMT arrays compared to single HEMT element are investigated. Figure 6 shows the HEMT array with N HEMTs, which can be fabricated on the same active layer and are with the same dimensional parameters with the HEMT described in previous section. The HEMT array period is set as d. It should be noted that, when computing the plasma oscillation in HEMT array and its THz radiation, the initial plasma oscillation phases between the HEMT elements are the same as each other.

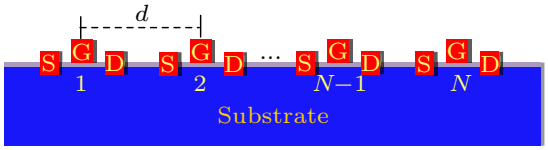


Fig. 6. The 2D model of the GaN HEMT array.

In order to calculate the theoretical directivity of the HEMT array antenna, supposing the array distribute along the z axis and the array center is set as the origin of the coordinates, the theoretical directivity of the N-element HEMT array

in spherical coordinates is computed as[31]

$$f_{\mathrm{T}}(\theta,\varphi) = f_{\mathrm{a}}(\theta,\varphi) f_{\mathrm{a}}(\theta,\varphi), \tag{4}$$

$$f_0(\theta,\varphi) = \sin(\theta), \tag{5}$$

$$f_{\mathrm{a}}(\theta,\varphi) = \sum_{n=1}^{N} \mathrm{e}^{\mathrm{j}(n-1)\psi}, \quad \psi = kd\cos\theta + \beta, \tag{6}$$

where, $f_0(\theta,\varphi)$ is the directivity function of the HEMT element, $f_{\mathrm{a}}(\theta,\varphi)$ is the array factor. In Eq. (6), ψ represents the phase difference of radiation field from adjacent elements to field point, k is electromagnetic wavenumber, d is array period, β is the initial phase difference of radiation field from adjacent elements to field point.

As for the two-element HEMT array, when the initial phases of 2DPs of the elements are the same, the theoretical radiation directivity diagram of HEMT array is shown in Fig. 7 with d changing from 5 μm ($\sim (1/8)\lambda$) to 40 μm ($\sim 1\lambda$). When d is shorter than 20 μm ($\sim (1/2)\lambda$), the main lobe become narrower with increasing the element spacing, when d is 40 μm, the side lobes are generated. It shows that enlarging the element spacing can improve the radiation directivity of the HEMT array but cannot enhance the radiation intensity at the maximum radiation direction of the array ($\theta = 90°$).

In the meanwhile, we also numerically obtain the 2D radiation field distribution in the whole air box. The radiation field amplitude distributions corresponding to different array period are shown in Fig. 8, when d varies from 5 μm to 40 μm, the main radiation energy concentrates in the narrower conical zones (the red zones) near the perpendicular bisector of HEMT array and the HEMT array behave as a broadside array antenna. When the element spacing is 40 μm, a fraction of radiation energy propagates in direction at a 45° angle to the array, which matches well with the theoretical formulas.

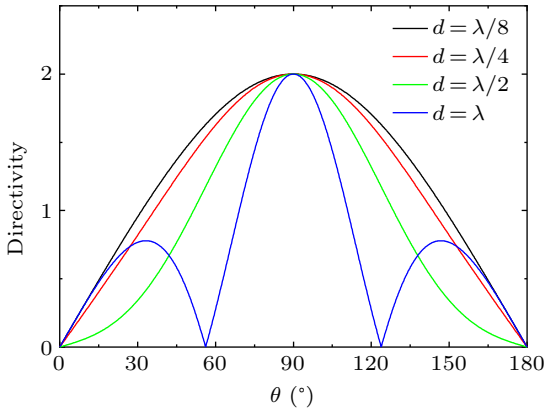


Fig. 7. The theoretical directivity diagram of two-element HEMT array corresponding to different array period d.

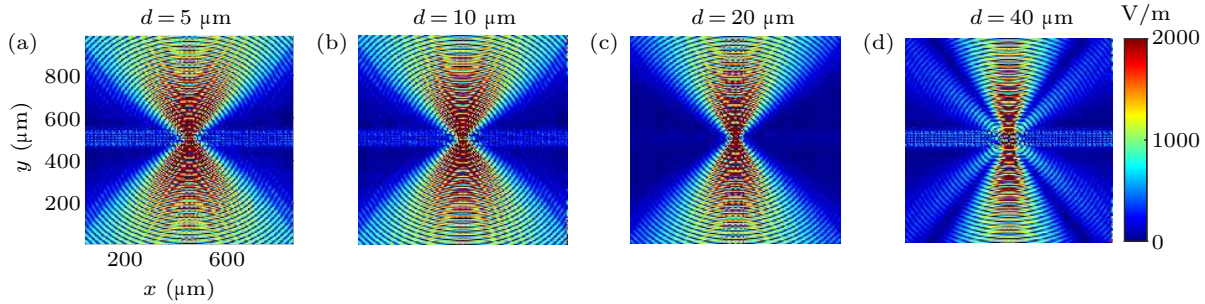


Fig. 8. The radiation electric field amplitude distributions of the two-element HEMT array when the array period d is 5 μm (a), 10 μm (b), 20 μm (c), 40 μm (d), respectively.

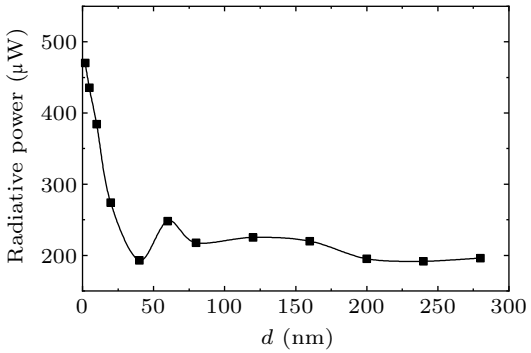


Fig. 9. The radiation power of the two-element HEMT array corresponding to different element spacing d.

As shown in Fig. 9, we simulated the radiation power of two-element HEMT array when unit spacing d increases from 2 μm to 160 μm, respectively. When d is 2 μm, the radiation power of the array is about four times of that of a single HEMT. When d varies from 2 μm to 40 μm, the radiation power drops from 470 μW to 210 μW. When d is larger than 40 μm, the radiation power of the array is about 210 μW, which is about 1.86 times that of a single HEMT unit. When d exceeds one THz radiation wavelength ($\sim$ 40 μm), the radiation power of the array stays around 200 μW. That is because d is so large that the two units of the array become almost independent on each other, and the power synthesis efficiency of the array becomes relatively poor. It shows that the radiation power of the array can be effectively improved by shortening the distance between the elements when the phases of the 2DP are synchronized.

As for the HEMT array with N elements, when the initial phases differences of the 2D plasmons of adjacent HEMT elements are zeros. As the distance between adjacent elements is fixed as 20 μm, according to Eq. (6), the radiation directivity

function of N-element HEMT array corresponding to different element number N is shown in Fig. 10. As N increases from 1 to 8, the radiation main lobe of the HEMT array gradually narrows and the radiation energy gradually concentrates in the area near the perpendicular bisector of the HEMT array. In addition, increasing the number of elements can greatly improve the power density at the strongest radiation direction of the array ($\theta = 90°$), which can both improve the radiation power of the array and make it easier to collect and utilize the radiation energy.

The numerical radiation electric field amplitude distribution of the N-element HEMT array is shown in Fig. 11. As the element number increases from 1 to 8, even though the side lobe number of HEMT array radiation increases, the radiation energy is concentrated in the narrower conical zones near the axis normal to the array. In other words, the radiation directivity become better and the radiation power is stronger as the element number is more. The numerical results also agree well with the theoretical prediction.

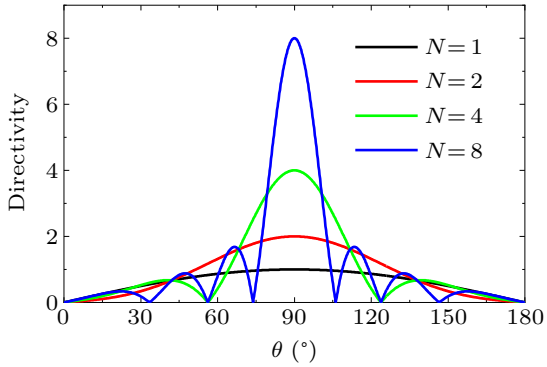


Fig. 10. Directivity diagram of the N-element HEMT array corresponding to different element number N.

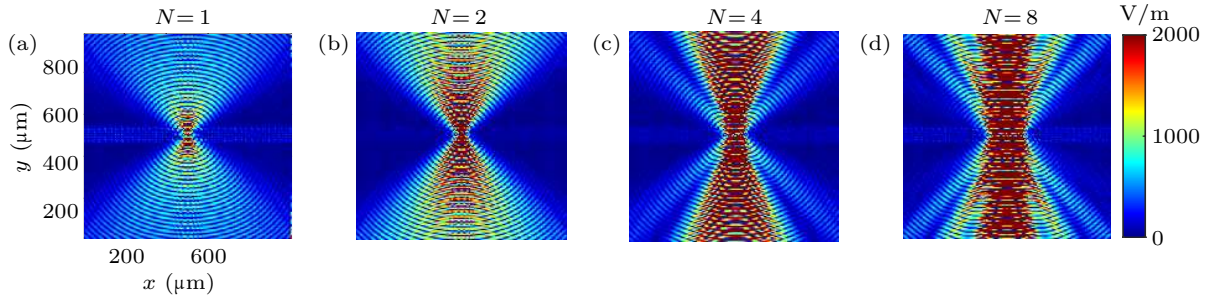


Fig. 11. The radiation electric field amplitude distributions of the HEMT array with the element numbers are 1 (a), 2 (b), 4 (c), and 8 (d), respectively.

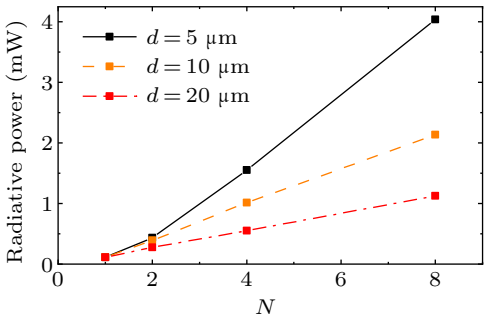


Fig. 12. The radiation power of the HEMT array corresponding to different element number N and array period d.

Then, we compared the radiation power of HEMT arrays under different unit number N corresponding to different array period d, as shown in Fig. 12, the black solid, yellow dashed, and red dashed–dotted lines represent the radiation powers corresponding to unit spacing $d = 5$ μm, 10 μm, and 20 μm, respectively. Along with the increase of N, the radiation power increases linearly. When d is 5 μm and N increased from 1 to 8, the radiation power of the array increases from 113 μW to 4 mW and increases by 35 times. When the spacing is 20 μm, the radiation power of the array is increased to 1.13 mW, which is increased by 10 times compared to single HEMT. That is to say, increasing the number of elements can effectively improve the radiation power of the array, and the narrower the unit spacing, the more significant the power improvement.

4. Plasmon phase synchronization in the GaN HEMT array induced by external Gaussian plane wave excitation

The radiation studies of HEMT arrays in the above sections are based on the premise that all HEMT elements are switched on simultaneously and the initial phases of the 2DPs within the elements are the same. However, in practice, even if all the elements are connected to the same voltage or current source, the phases of the 2DPs among the units are still random. The theoretical radiation directivity of the two-element array when the phases of the plasma waves in the two HEMTs are synchronous and asynchronous are compared, as shown in Fig. 13. It shows that when the plasma wave phases between the two units are asynchronous, the main radiation direction of the array deviated from the perpendicular of the array ($\theta = 90°$), and the overall radiation intensity is lower than that of the array with synchronous phases.

We compared the radiation field distribution and the radiation power of the two-element HEMT array when the initial phases of 2DPs are synchronous and asynchronous (phase difference of 115°), as shown in Fig. 14. When the plasmon

phase of the elements is synchronous, the radiated power of the array is mainly concentrated near the vertical line of the array. However, when the phase is asynchronous, the main radiated direction deviates much from the vertical direction of the array, which is in good agreement with the theoretical prediction. We then compared the radiated power of the HEMT array with and without phase synchronization in the array. As shown in Fig. 14(c), the radiation frequency of the two arrays are both 6.77 THz when the element phase is synchronous and asynchronous. The array radiation power is 277 μW when the 2DPs' phases are synchronous and 197 μW when the 2DPs' phases are asynchronous. In other words, compared to the synchronous plasmon phase, the asynchronous plasmon will significantly weaken the radiated power of the HEMT array.

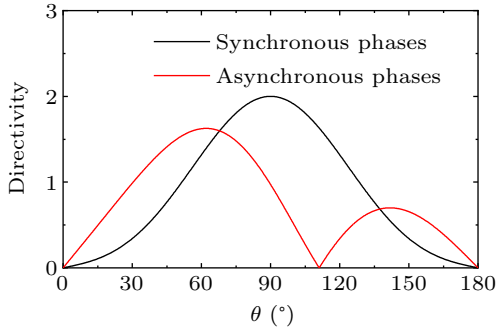


Fig. 13. Radiation directivities of two-element HEMT array with synchronous (black line) and asynchronous (red line) 2DPs' phases.

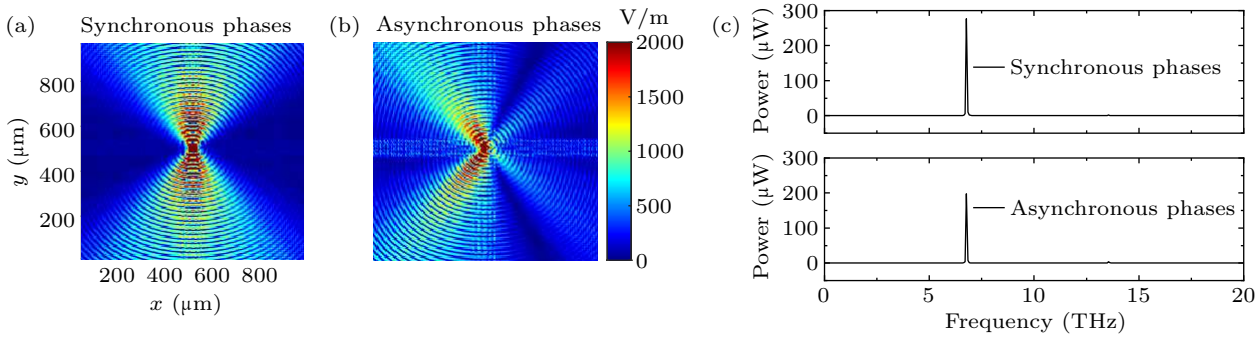


Fig. 14. Radiation electric field amplitude distribution of two-element HEMT array with synchronous (a) and asynchronous (b) 2DPs' phases, respectively; (c) radiation power spectrums of fields in panels (a) and (b).

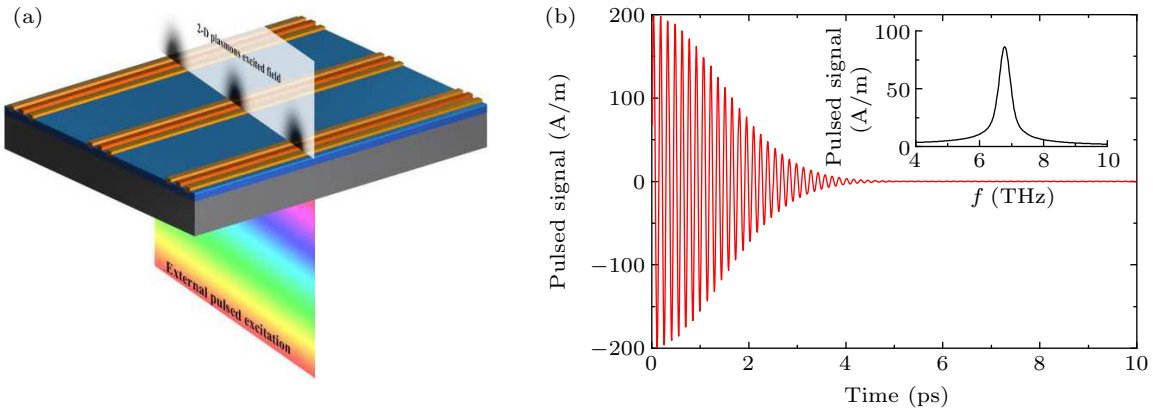


Fig. 15. The schematic diagram of HEMT array with external Gaussian plane wave excitation (a) and the temporal dependence of the Gaussian signal (b).

Since the asynchronous plasmon phase between the elements in the HEMT array will lead to the reduction of the radiation power, we adopt the external pulse excitation to synchronize the random plasmon phase in the array. The specific implementation is that a Gaussian plane wave with frequency the same as the plasmon resonance is vertically incident below the array. This signal travels through the HEMT array and interacts with the plasma wave inside the HEMT and eventually force the phases of the plasmons in different units to become synchronized, which is similar to phase-locking in communication field. The setup schematic including the HEMT array, external plane wave excitation and surface wave distribution generated by HEMT array are shown in Fig. 15(a). The time-decayed Gaussian signal is adopted as the external excitation source and the time-varying curve of the Gaussian signal is shown in Fig. 15(b). The central frequency of the Gaussian signal is 6.8 THz and the signal duration is about 5 ps. The Fourier transform of the Gaussian signal is shown in the inset of Fig. 15, the bandwidth of the signal is about 500 MHz.

We then compare the plasmon resonance in the HEMT element with and without introducing the Gaussian signal. As control, three HEMTs in which the plasma wave is excited

at 1 ps, 1.1 ps, and 1.2 ps are respectively studied and the structural parameters and working conditions of these three HEMTs are the same as those of the above section. The temporal dependence of the source current in the first 10 ps and the last 2 ps in these three HEMTs are shown in Figs. 16(a) and 16(b). The phases of plasma wave in the second and third HEMTs are 115° behind and 130° ahead of the plasma wave in the first HEMT. It shows that the phases of the source current in the three HEMT units are asynchronous in the whole computational process. On the other hand, as shown in Fig. 16(c) and 16(d), after introducing the Gaussian pulse, the phase synchronization between different units are established after 2.5-ps moment and the phase-synchronization continues until the end. In other words, applying a planar electromagnetic pulse with the same resonant frequency as the HEMT plasma wave can synchronize the phases of the plasma waves in the HEMT array, which can maximize the radiation power of the HEMT array.

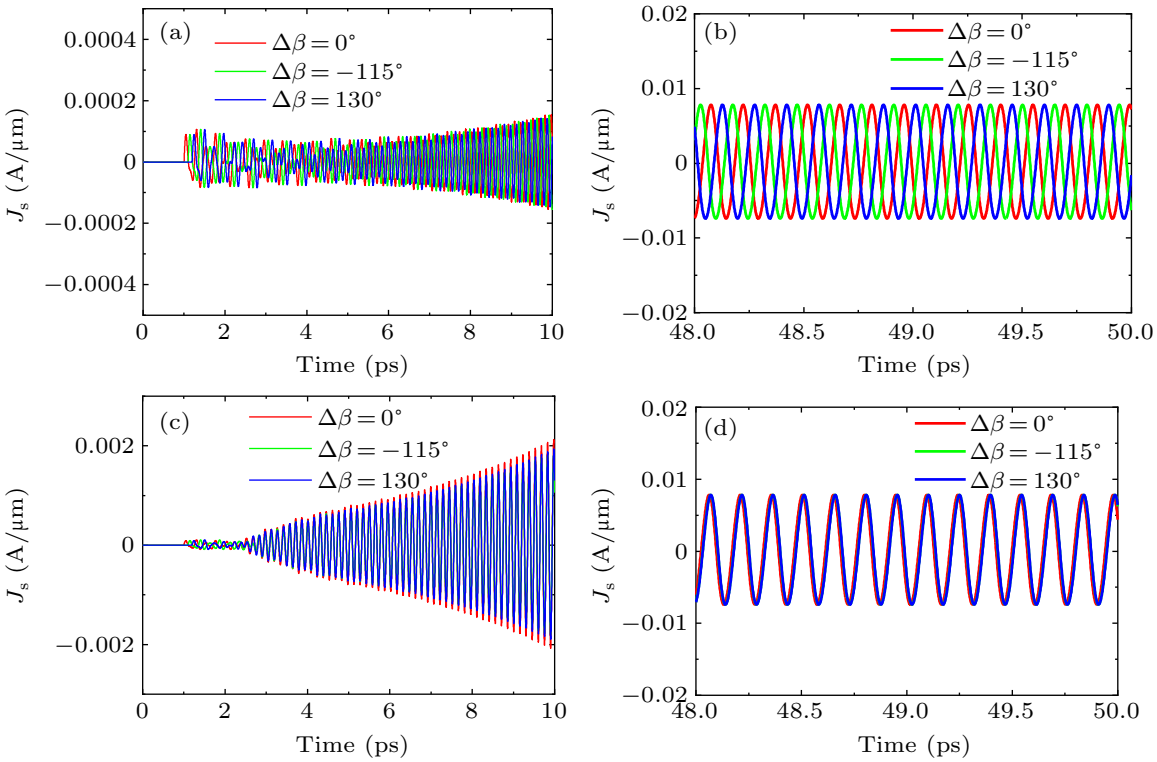


Fig. 16. The temporal dependences of the areal source currents in the first 5 ps and the last 2 ps when the initial phase difference of the plasma wave is 0°, −115°, and 130° in the HEMT element; panels (a) and (b) and panels (c) and (d) represent the source currents without and with Gaussian plane wave excitation, respectively.

5. Conclusion

In this work, plasma instability in 2DEG of GaN HEMT and the radiation power amplification of 1D HEMT array compared to the single HEMT have been investigated. Under the DS boundary condition, plasma instability and 2D plasmon resonance are generated in the 2DEG in the HEMT. The temporal and spatial distributions of the alternative sheet current in the channel were analyzed and the distribution of the excited electric field inside the HEMT and in the space of several radiation wavelengths were obtained. Then, several HEMT elements were periodically integrated as a 1D array in the same active layer, the working conditions of all the HEMT units and the initial phases of the 2DPs among the elements in the array are both set as the same. The power amplification and radiation directivity of the HEMT array with different array periods and numbers have been studied. It was found that the radiation directivity of HEMT array is very close to the radiation characteristic of element antenna array. Increasing element spacing can narrow the radiation main lobe width but reduce the radiation power of array, while increasing the elements number can both effectively improve the radiation directivity and radiation power of array. In addition, in order to overcome the radiation power degradation caused by the phase asynchronism in the plasma waves in HEMT array, an external Gaussian plane wave excitation method is applied to interact with the plasma waves in the array and eventually synchronizes the plasmon phases. Our quantified numerical analysis on the power amplification and radiation directivity of the HEMT array provides a useful guidance for THz radiation devices based on 2D-plasmon resonance in semiconductor devices.

Acknowledgment

Project supported by the National Natural Science Foundation of China (Grant Nos. 92163204, 61921002, and

62171098).

References

[1] Siegel P H 2002 *IEEE T. Microw. Theory* **50** 910
[2] Liu S 2006 *China Basic Science* **7** (in Chinese)
[3] Dhillon S S, Vitiello M S, Linfield E H, *et al.* 2017 *J. Phys. D* **50** 043001
[4] Tonouchi M 2007 *Nat. Photon.* **1** 97
[5] Lewis R A 2014 *J. Phys. D* **47** 374001
[6] Allen S J, Tsui D C and Logan R A 1977 *Phys. Rev. Lett.* **38** 980
[7] Gornik E and Tsui D C 1976 *Phys. Rev. Lett.* **37** 1425
[8] Shur M S 2021 *IEEE Sens. J.* **21** 12752
[9] Otsuji T and Shur M 2014 *IEEE Microw. Mag.* **15** 43
[10] Dyakonov M and Shur M 1993 *Phys. Rev. Lett.* **71** 2465
[11] Knap W, Lusakowski J, Parenty T, *et al.* 2004 *Appl. Phys. Lett.* **84** 2331
[12] Lusakowski J, Knap W, Dyakonova N, *et al.* 2005 *J. Appl. Phys.* **97** 064307
[13] Boubanga-Tombet S, Teppe F, Torres J, *et al.* 2010 *Appl. Phys. Lett.* **97** 262108
[14] Zhou Y, Li X, Tan R, *et al.* 2013 *J. Semicond.* **34** 022002
[15] Jakštas V, Grigelionis I, Janonis V, *et al.* 2017 *Appl. Phys. Lett.* **110** 202101
[16] Shalygin V, Moldavskaya M, Vinnichenko M, *et al.* 2019 *J. Appl. Phys.* **126** 183104
[17] Meziani Y M, Otsuji T, Hanabe M, *et al.* 2007 *Appl. Phys. Lett.* **90** 061105
[18] Meziani Y M, Handa H, Knap W, *et al.* 2008 *Appl. Phys. Lett.* **92** 201108
[19] Watanabe T, Satou A, Suemitsu T, *et al.* 2013 *CLEO*: 2013, June 9–14, 2013, San Jose, California, pp. 1–2
[20] Hosotani T, Satou A and Otsuji T 2021 *Appl. Phys. Express* **14** 051001
[21] Aizin G R, Mikalopas J and Shur M 2016 *Phys. Rev. B* **93** 195315
[22] Shur M and Gaska R (US patent) 7638817 B2 [2009-10-29]
[23] Elkhatib T A, Kachorovskii V Y, Stillman W J, *et al.* 2010 *IEEE Trans. Microw Theor. Tech.* **58** 331
[24] Popov V V, Tsymbalov G M, Fateev D V, *et al.* 2006 *Appl. Phys. Lett.* **89** 123504
[25] Bhardwaj S, Nahar N K, Rajan S, *et al.* 2016 *IEEE Trans. Electron. Dev.* **63** 990
[26] Nafari M, Aizin G R and Jornet J M 2018 *Phys. Rev. Appl.* **10** 064025
[27] Ardaravičius L, Matulionis A, Liberis J, *et al.* 2003 *Appl. Phys. Lett.* **83** 4038
[28] Dmitriev A P, Furman A S and Kachorovskii V Y 1996 *Phys. Rev. B* **54** 14020
[29] Dyakonov M and Shur M S 2005 *Appl. Phys. Lett.* **87** 111501
[30] Zhang Y and Shur M S 2020 *IEEE Trans. Electron. Dev.* **67** 4858
[31] Balanis C A 2005 *Antenna Theory Analysis and Design*, 4th edn. (Hoboken, New Jersey.: John Wiley & Sons, Inc.) pp. 285–384